Evaluation of phase-shifting techniques for a self-referencing interferometer wavefront sensor (Postprint)

Melissa S. Corley and Troy A. Rhoadarmer

29 July 2005

Conference Proceedings

APPROVED FOR PUBLIC RELEASE; DISTRIBUTION IS UNLIMITED.

AIR FORCE RESEARCH LABORATORY
Directed Energy Directorate
3550 Aberdeen Ave SE
AIR FORCE MATERIEL COMMAND
KIRTLAND AIR FORCE BASE, NM 87117-5776

REPORT DOCUMENTATION PAGE

Public reporting burden for this collection of information is estimated to average 1 hour per response, including the time for reviewing instructions, searching existing data sources, gathering and maintaining the data needed, and completing and reviewing this collection of information. Send comments regarding this burden estimate or any other aspect of this collection of information, including suggestions for reducing this burden to Department of Defense, Washington Headquarters Services, Directorate for Information Operations and Reports (0704-0188), 1215 Jefferson Davis Highway, Suite 1204, Arlington, VA 22202-4302. Respondents should be aware that notwithstanding any other provision of law, no person shall be subject to any penalty for failing to comply with a collection of information if it does not display a currently valid OMB control number. **PLEASE DO NOT RETURN YOUR FORM TO THE ABOVE ADDRESS.**

1. REPORT DATE (DD-MM-YYYY) 29-07-2005	2. REPORT TYPE Conference Proceedings		3. DATES COVERED (From - To) 1 Apr 02 – 1 Jul 04
4. TITLE AND SUBTITLE Evaluation of phase-shifting techniques for a self-referencing Interferometer wavefront sensor (Postprint)			5a. CONTRACT NUMBER In House – 299962
			5b. GRANT NUMBER
			5c. PROGRAM ELEMENT NUMBER 063605F
6. AUTHOR(S) Melissa S. Corley, Troy A. Rhoadarmer			5d. PROJECT NUMBER JT00
			5e. TASK NUMBER S0
			5f. WORK UNIT NUMBER AB
7. PERFORMING ORGANIZATION NAME(S) AND ADDRESS(ES) AFRL/DESE 3550 Aberdeen Ave SE Kirtland AFB, NM 87117-5776			8. PERFORMING ORGANIZATION REPORT NUMBER
9. SPONSORING / MONITORING AGENCY NAME(S) AND ADDRESS(ES) AIR FORCE RESEARCH LABABATORY 3550 Aberdeen Ave SE Kirtland AFB, NM 87117-5776			10. SPONSOR/MONITOR'S ACRONYM(S) AFRL/DESE
			11. SPONSOR/MONITOR'S REPORT NUMBER(S) AFRL-DE-PS-TP-2007-1009

12. DISTRIBUTION / AVAILABILITY STATEMENT

Approved for Public Release; Distribution is Unlimited.

14. ABSTRACT
The Air Force Research Laboratory is developing a Self-Referencing Interferometer (SRI) wavefront sensor (WFS) for applications requiring laser propagation in strong scintillation. This paper compares several phase-shifting techniques that can be used to capture interference patterns and examines their effects on SRI WFS performance. These techniques included temporal, spatial, spatial-temporal phase shifting. Temporal phase shifting allows for straightforward setup, alignment, and calibration, though its performance is degraded by changes in the atmosphere between measurements. Spatial phase shifting effectively "freezes" the atmosphere, but required more rigorous camera calibration and alignment. Spatial-temporal phase shifting balances the benefits and challenges of both methods. This paper includes a discussion of the tradeoffs involved in selecting an appropriate phase-shifting approach for a given application. Laboratory results demonstrate the advantages and disadvantages of each technique in evaluation of SRI WFS performance.

15. SUBJECT TERMS
Adaptive optics, wave front sensors, phase shifting interferometer, scintillation.

16. SECURITY CLASSIFICATION OF:			17. LIMITATION OF ABSTRACT	18. NUMBER OF PAGES	19a. NAME OF RESPONSIBLE PERSON Melissa Corley
a. REPORT Unclassified	b. ABSTRACT Unclassified	c. THIS PAGE Unclassified	SAR	14	19b. TELEPHONE NUMBER (include area code)

Evaluation of phase-shifting techniques for a self-referencing interferometer wavefront sensor

Melissa S. Corley and Troy A. Rhoadarmer

Optics Division, AFRL/DES, Directed Energy Directorate,
U.S. Air Force Research Laboratory, Kirtland AFB, NM 87117-5776 USA

ABSTRACT

The Air Force Research Laboratory is developing a Self-Referencing Interferometer (SRI) wavefront sensor (WFS) for applications requiring laser propagation in strong scintillation. This paper compares several phase-shifting techniques that can be used to capture interference patterns and examines their effects on SRI WFS performance. These techniques include temporal, spatial, and spatial-temporal phase shifting. Temporal phase shifting allows for straightforward setup, alignment, and calibration, though its performance is degraded by changes in the atmosphere between measurements. Spatial phase shifting effectively "freezes" the atmosphere, but requires more rigorous camera calibration and alignment. Spatial-temporal phase shifting balances the benefits and challenges of both methods. This paper includes a discussion of the tradeoffs involved in selecting an appropriate phase-shifting approach for a given application. Laboratory results demonstrate the advantages and disadvantages of each technique in evaluation of SRI WFS performance.

Keywords: adaptive optics, wave front sensors, phase-shifting interferometer, scintillation

1. INTRODUCTION

The wavefront sensor (WFS) is an integral part of an adaptive optics (AO) system. The performance of the WFS directly influences the achievable AO system Strehl ratio. While many current AO systems utilize a Shack-Hartmann WFS or a lateral shearing interferometer (LSI) to estimate wavefront aberrations, branch points in the wavefront phase degrade the performance of these systems in the presence of strong scintillation.[1-3] To operate in extended turbulence conditions, an alternative system is being developed to improve wavefront estimation accuracy.

The Air Force Research Laboratory Directed Energy Directorate's Starfire Optical Range (SOR) has been developing an innovative WFS technology that will improve WFS performance in strong scintillation – the self-referencing interferometer (SRI).[4-6] The performance of this WFS is theoretically immune to scintillation. A summary of its theory of operation and analysis of predicted performance can be found in previous conference papers.[4-6] Tests of the SRI WFS are currently underway in the SOR's Atmospheric Simulation and Adaptive-optics Laboratory Testbed (ASALT). This paper presents some results from those tests. A conceptual description of SRI operation is summarized in Section 2, and comparison and description of four phase-shifting methods follow in Section 3. Lab setup and a phase-shift experiment are described in Section 4, and laboratory test results from the phase-shift experiment are presented in Section 5.

2. OVERVIEW OF THE SRI WFS

The SRI WFS is based on a phase-shifting, point diffraction interferometer. Additional theory of phase shifting for a point-diffraction interferometer has been published in a previous paper.[6] Figure 1 shows a conceptual diagram of the SRI WFS. When the optical field enters the system, a beamsplitter divides it into a beacon beam and a reference beam. The reference beam is coupled into a single mode fiber, where it passes through an optical amplifier and an inline phase shifter. The fiber spatially filters the reference beam and produces a known field at the fiber output, while the phase shifter controls the phase of the beam. The beacon and reference beams recombine at the WFS camera to produce interferometric fringes. The WFS camera measures the integrated fringe intensity over each WFS subaperture. The optical amplifier is used to increase the amplitude of the fringes by boosting the power on the reference beam.
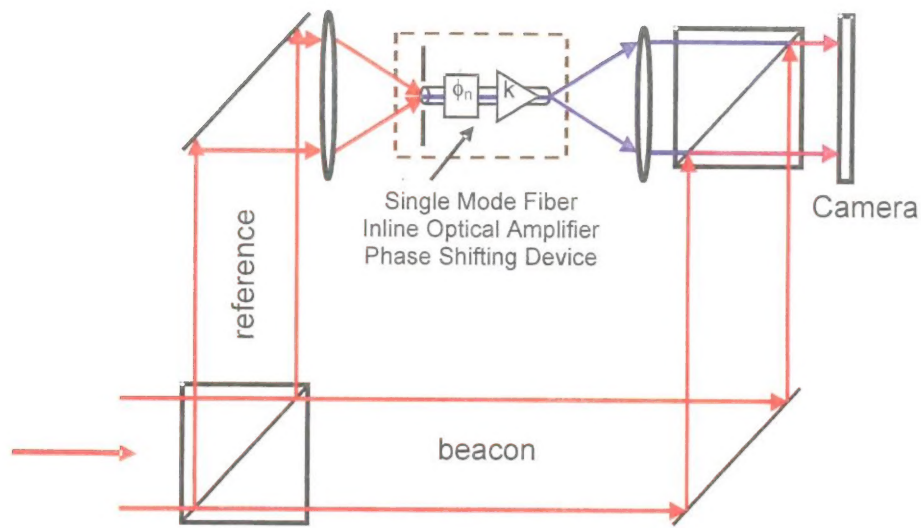
Figure 1. Conceptual diagram of the SRI WFS.

It can be shown that the SRI WFS measures the average optical field of the beacon over each subaperture and that the amplitude and phase of the field can be estimated from the intensities derived from shifting the phase of the reference beam.[4,7] The estimated beacon phase can be used to close an AO loop by aligning the actuators of a deformable mirror (DM) to the subaperture centers of the SRI WFS. Because the SRI WFS directly measures the average field of the beacon wavefront, it can be shown that, in the absence of noise, the SRI WFS's estimation of the beacon field in Kolmogorov turbulence depends only on the ratio of the actuator size (d) to the atmospheric coherence length (r_0).[4] In contrast to the Shack-Hartmann WFS and LSI, the performance of the SRI WFS does not depend on scintillation. Therefore, in strong scintillation, the SRI WFS should outperform systems using Shack-Hartmann and LSI wavefront sensing and estimation methods.

3. PHASE SHIFTING TECHNIQUES

To determine wavefront phase, a minimum of three measurements is necessary to solve for the three unknowns of reference beam amplitude, beacon beam amplitude, and wavefront phase difference. Using the measured intensities from three phase shifts on the reference beam, the amplitude and phase of the beacon field can be estimated. While using three phase shifts is sufficient, four are more often used for ease of computation, most efficient use of light, and noise mitigation.[7] Figure 2 shows four phase-shifted images. For clarity in viewing the phase-shifted fringes, these images are captured from a clean reference beam that does not travel through turbulence. The interference fringes are noticeably shifted from one image to the next.
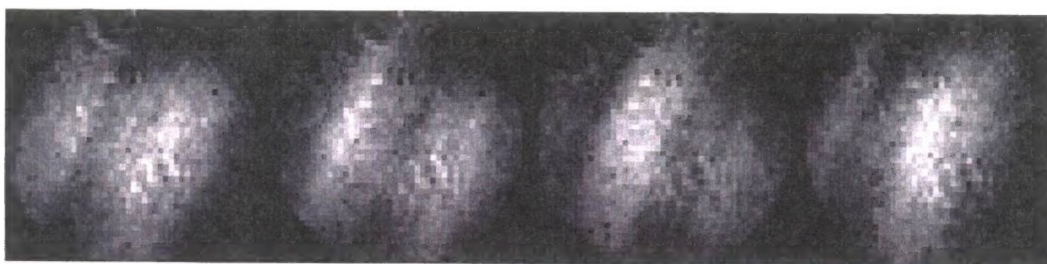

Figure 2. 4-bin phase shift example. From left to right, images have phase shifts of $\theta_n = \{0, 90, 180, 270\}$ degrees.

The two primary categories of phase-shifting techniques are spatial and temporal. A third method, spatial-temporal, combines these methods and incorporates the advantages and disadvantages of both. There are several trades to consider when choosing a phase-shifting technique. The methods and their characteristics are discussed below.

3.1 Spatial phase shifting

In spatial phase shifting, both of the output beams from the last beamsplitter shown in Fig. 1 are further split into two beams. The four resulting beams are then phase-shifted using static optics to create equally spaced phase shifts of $\theta_n = \{0, 90, 180, 270\}$ degrees. After the beams are recombined, the four interference patterns are imaged simultaneously. The images can be sent to four separate detectors or to four quadrants of one detector. Figure 3 shows a conceptual schematic of the four images produced by the spatial phase-shifting method. The measured intensities from each phase shift on the reference beam are determined by:[7]

$$I_n = I_{ref} + I_{beacon} + 2\sqrt{I_{ref} \, I_{beacon}} \; \cos[\phi_{beacon} + \theta_n],$$ (1)

where I_{ref} is the intensity of the reference beam, I_{beacon} is the intensity of the beacon beam, ϕ_{beacon} is the phase of the beacon beam, and θ_n is the phase of the reference beam. For the phase-shift algorithm, wavefront phase can be determined using the measured intensities corresponding to the four phase shifts as follows:[7]

$$\phi(x, y) = \tan^{-1}\left[\frac{I_4 - I_2}{I_1 - I_3}\right],$$ (2)

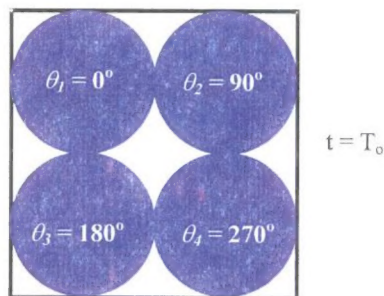where the phase output from the arctangent is between $-\pi$ and π.

Figure 3. Spatial phase-shift method. All four phase-shifted images are taken at the same time.

Spatial phase shifting offers the advantage of capturing all images at the same time, thus avoiding any change in the wavefront from one interference measurement to the next, as could happen if data were taken temporally. It effectively "freezes" the atmosphere in time, allowing for a more accurate phase reconstruction of the wavefront with respect to a changing atmosphere. While alignment is difficult for hardware implementing spatial phase shifting, one benefit is that once set up, the hardware can be very stable. Once it has been aligned, it will produce the same phase shifts every time. Therefore, it is possible to implement phase shifts of 90 degrees more stably than with temporal methods.

However, spatial phase shifting requires more complex calibration, alignment, and hardware setup compared to temporal methods. If multiple cameras are used, cost and bench space could quickly become limiting factors in the system layout. At the same time, using a single camera may decrease the resolution possible in the interference images; all four must fit on one detector. Additionally, co-aligning the beams on the detectors and maintaining the proper phase shifts between the images requires very complex hardware. It is also necessary to calibrate the detectors so that gain and bias variations between detectors can be accounted for. These variations must be corrected before the measurements are combined to estimate the wavefront. Finally, since multiple beam paths exist in space, non-common path aberrations may corrupt the wavefront estimation process.[5]

3.2 Temporal phase shifting

In temporal phase shifting, three or four interferograms are imaged onto the same detector but spaced apart in time over consecutive integration periods.[4] Figure 4 illustrates this method. The effective measurement time, T_o, is centered between the images, and the time and phase shift associated with each image are shown in the figure. The 4-bin method has a larger effective latency compared to spatial phase shifting by a frame and a half, while the 3-bin method has a larger effective latency by a frame. Therefore, the 3-bin algorithm has a smaller effective latency compared to the 4-bin algorithm.[7] However, due to coherent noise and vibrations, the 3-bin algorithm is more sensitive to phase-shift errors than the 4-bin algorithm.

4-bin   **3-bin**

$t = T_o - {}^3/_2\Delta T,\ \theta_1 = 0°$

$t = T_o - {}^1/_2\Delta T,\ \theta_2 = 90°$

$t = T_o + {}^1/_2\Delta T,\ \theta_3 = 180°$

$t = T_o + {}^3/_2\Delta T,\ \theta_4 = 270°$

$t = T_o - \Delta T,\ \theta_1 = 0°$

$t = T_o,\ \theta_2 = 120°\ \ (90°)$

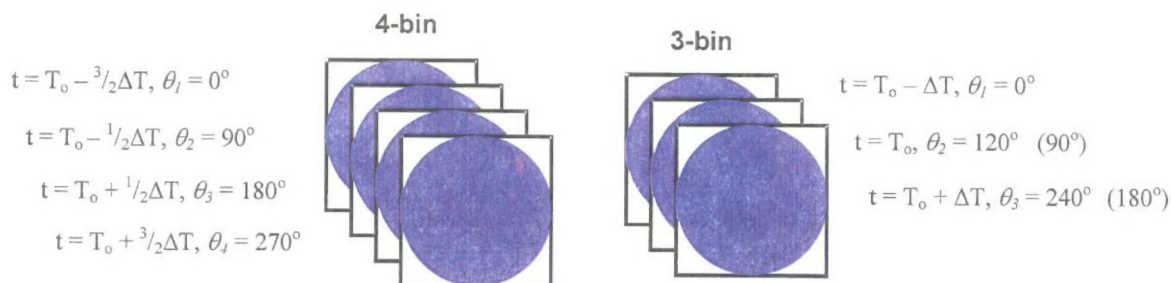$t = T_o + \Delta T,\ \theta_3 = 240°\ \ (180°)$

Figure 4. Temporal phase-shift methods. (a) 4-bin algorithm – four interference patterns are imaged sequentially in time, and (b) 3-bin algorithm – three interference patterns are imaged sequentially in time. The 3-bin algorithm can be implemented using phase shifts of 90 degrees or 120 degrees. ΔT is the camera framing interval.

The 4-bin algorithm uses Equation (2) with four phase shifts spaced 90 degrees apart. There are various ways to implement the 3-bin algorithm, but the two most common utilize phase shifts of 120 degrees and 90 degrees. For 120-degree phase shifts, $\theta_n = \{0, 120, 240\}$ degrees, and the wavefront phase using three intensity measurements can be determined as:

$$\phi(x, y) = \tan^{-1}\left[\sqrt{3}\,\frac{I_1 - I_3}{2I_2 - I_1 - I_3}\right]. \tag{3}$$

Similarly, for 90-degree phase shifts, $\theta_n = \{0, 90, 180\}$ degrees, and with three intensity measurements, the wavefront phase can be determined as:[7]

$$\phi(x, y) = \tan^{-1}\left[\frac{I_1 - I_3}{2I_2 - I_1 - I_3}\right]. \tag{4}$$

The algorithms described are equivalent to a least-squares solution for determining the wavefront. Each of these algorithms can be implemented by capturing all new frames for every wavefront reconstruction or by using a "sliding window" approach. In the former method, a new set of three or four images is captured before the wavefront aberrations are estimated and the DM is updated. Using a sliding window approach, the most recent frames can be used and the DM can be updated after every frame; the reconstructions "slide" with each frame rather than "jumping" from one set to the next. For example, if the first reconstruction utilizes frames 1, 2, 3, and 4, the sliding window method will implement the next reconstruction using frames 2, 3, 4, and 5. With the non-sliding window approach, the next reconstruction would wait for frames 5, 6, 7, and 8. Some measurement degradation is possible using the sliding window approach as the simulated atmosphere and the DM both change between each measurement. However, this approach allows for closer tracking of the atmospheric effects because it does not wait for all new frames before updating the DM.

Temporal phase shifting allows for much simpler hardware and calibrations than spatial phase shifting. Because temporal phase shifting uses a shift in time rather than space, it requires minimal hardware and allows for lower system cost. One detector will suffice, and the resolution does not suffer from splitting the image into quadrants on the same

detector. Therefore, for a given detector size, better resolution is possible with temporal phase shifting than with spatial. Even if the detector is operated with the same resolution as with spatial phase shifting, temporal can provide more photons in each measurement because the beam is not divided as many times. This improves signal-to-noise ratio and performance.[4] Co-alignment and camera calibration are also not as difficult as with spatial phase shifting, and each measurement will have the same gain and bias. Finally, non-common path aberrations from multiple beams are mitigated, as there is only one beam path.

While there are many benefits of using temporal phase shifting rather than spatial, temporal phase shifting does present its own challenges. The main drawback of using temporal phase shifting is the turbulent nature of the atmosphere.[4-7] Because atmospheric turbulence is dynamic, the field in each subaperture can change from one interference measurement to the next. Therefore, the field and even the deformable mirror may not be constant over all the WFS measurements as they are for images taken simultaneously, and this will corrupt wavefront estimation. Detailed analysis of the magnitude of amplitude and phase change is developed in a previous paper.[5] Furthermore, since only one beam is imaged in temporal phase shifting, half the light from the original field is lost at the last beamsplitter shown in Fig. 1. Finally, with a dynamic fiber phase shifter, calibration and drift become problems. The phase shifter must be calibrated as described in Section 3.4 to reduce phase-shift errors. The fiber phase shifter is also susceptible to drift from hysteresis in its actuator as well as from laboratory turbulence.

3.3 Spatial-temporal phase shifting

In spatial-temporal phase shifting, two images are taken simultaneously and imaged onto two detectors or two quadrants of one detector. The images are obtained from the two output beams from the last beamsplitter shown in Fig. 1. The two images have a 180-degree phase shift between them ($0°$ and $180°$). In the next integration period, the inline fiber phase shifter is used to shift the reference by 90 degrees, producing the two remaining interference patterns that complete the 4-bin set ($90°$ and $270°$). Figure 5 illustrates this method. The 4-bin algorithm in Equation (2) can then be used to reconstruct the wavefront phase. It is also possible to use the sliding window approach described in Section 3.2 in implementing the algorithm. Once again, the effective measurement time is centered between the two images, and effective latency is half a frame larger than with spatial phase shifting.

$t = T_o - \frac{1}{2}\Delta T$
$\theta_1 = 0°, \theta_3 = 180°$

$t = T_o + \frac{1}{2}\Delta T$
$\theta_2 = 90°, \theta_4 = 270°$

Camera 2
$|U_b + U_r e^{i(\pi+\theta\eta)}|^2$
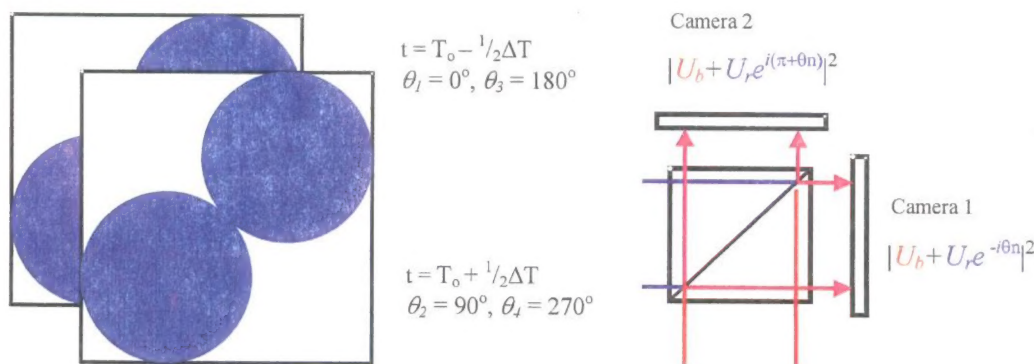
Camera 1
$|U_b + U_r e^{-i\theta\eta}|^2$

Figure 5. Spatial-temporal phase-shift method. Two images are taken simultaneously with a 180-degree phase shift between them and imaged onto two detectors. ΔT is the camera framing interval.

Considering the advantages and disadvantages of spatial and temporal phase shifting, it may be beneficial to combine the methods to utilize the strengths of both. Spatial-temporal phase shifting blends the effects of the inherent static and dynamic properties of propagation and the atmosphere. Compared to temporal phase shifting, taking two images at a time for two integration periods reduces the atmospheric distortion of the phase measurement due to turbulence, and compared to spatial phase shifting, splitting the images onto two detector arrays instead of four decreases path aberrations and co-alignment difficulties. Furthermore, spatial-temporal phase shifting can use all the light from the original field. Unlike temporal phase shifting, both beams coming out of the last beamsplitter are imaged onto cameras, as shown in Fig. 5. The second image is effectively "free" and will be there whether it is captured or not, so the spatial-temporal method takes advantage of this and provides more efficient use of the light. For a given detector size, spatial-temporal phase shifting achieves better resolution compared to spatial, but achieves less resolution

compared to temporal. This method presents a middle ground from which to balance hardware and calibration complexity, performance loss due to dynamic atmospheric turbulence, and efficient use of light while still forming four images to solve for wavefront phase.

3.4 Phase-Shift Calibration

When using a fiber phase shifter or similar hardware, all the methods above require an initial calibration between phase-shift angle and the recorded interferograms to minimize errors in the phase shift. For the more sensitive ones such as the 3-bin temporal algorithm using 90-degree phase shifts, this calibration is more critical. However, proper phase-shift calibration improves the performance of each method.[7] The phase-shift calibration method used in SOR laboratory investigations records four interference patterns with equal phase steps and calculates the phase shift at each measurement point using the Carré algorithm.[7] The calibration routine runs within closed loop control, adjusting the phase shift until a target phase shift is achieved.

3.5 Phase unwrapping

An additional factor to consider in SRI WFS operation is phase unwrapping. The phase from the arctangent is limited to be between $-\pi$ and π. If the deformable mirror is a continuous surface, the phase must be unwrapped to form a continuous solution with phase resets removed. A least-squares phase unwrapping approach is used in the laboratory tests discussed in this paper to unwrap the wavefront phase.

A better phase reconstruction can be achieved by including not only the least-squares unwrapped phase, but also the branch-point phase contribution. The SRI WFS can be used to introduce branch cuts and solve for the branch-point phase contribution. When d/r_0 is on the order of 1 or greater, tilt across a subaperture has reasonable probability to exceed 2π. In this case, the average field in the subaperture can become zero, and the SRI WFS may artificially indicate the presence of a branch point in the subaperture. In the experiments described in this paper, only the least-squares method was used. We are currently developing the most optimal ways to include the branch-point contribution.

3.6 WFS resolution

Analysis in a previous conference paper has shown that the SRI WFS is more sensitive to large tilts than the Hartmann WFS, particularly when introducing branch cuts on a continuous-surface DM to solve for the branch-point phase contribution.[4] To handle the problem of large tilts, a WFS of higher resolution can be used. A high-resolution SRI WFS over-samples the wavefront and has a 2 x 2 or larger block of subapertures for each DM actuator. A comparison of high-resolution and low-resolution subaperture-actuator layouts is shown in Figure 6. With the larger subaperture block, d/r_0 decreases, allowing SRI WFS performance to increase. One possible drawback of this implementation is that while there are more subapertures in the high-resolution case, the number of DM actuators remains the same. Consequently, while the high-resolution WFS can make better measurements, the overall system may not be able to use all of this high-resolution potential when fitting the DM. A more effective way to increase resolution may be to increase the number of DM actuators in addition to the number of subapertures. However, increasing resolution as described is not always possible. Higher resolution has shown some better performance in laboratory tests, and other methods are under additional study to improve SRI WFS performance.
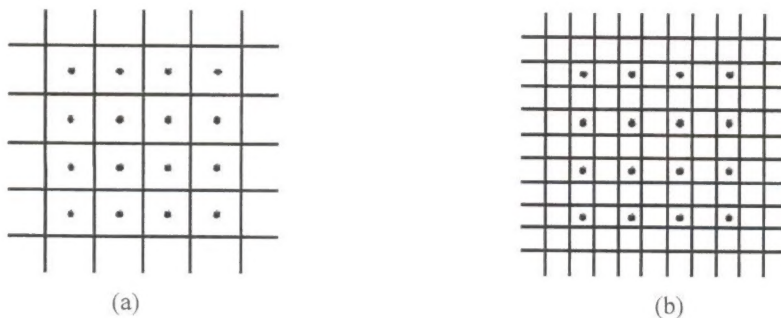

(a)   (b)

Figure 6. (a) A 1-to-1 correspondence between WFS subapertures and DM actuators. Actuators are denoted by dots and subapertures by squares. (b) A high-resolution layout – two subapertures per actuator spacing.
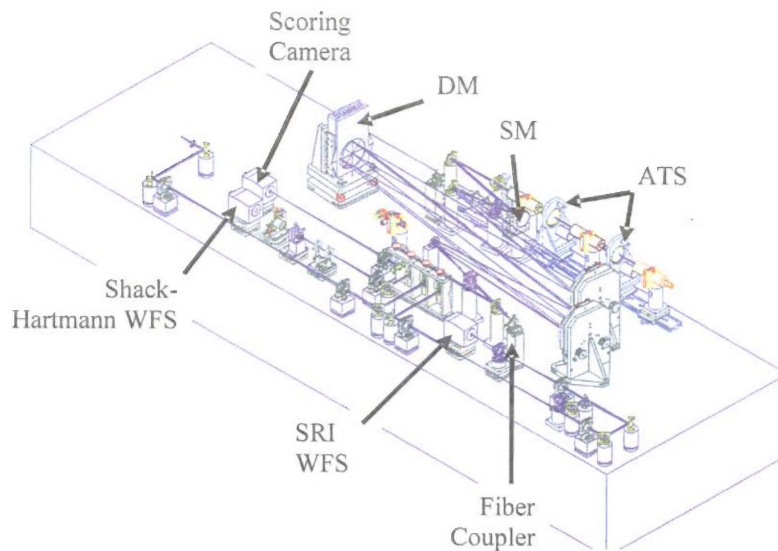
Figure 7. Hardware and optical layout of ASALT Laboratory.

4. LABORATORY EXPERIMENT DESCRIPTION

The SOR's Atmospheric Simulation and Adaptive-optics Laboratory Testbed (ASALT) provides a breadboard setting in which to increase our understanding of SRI WFS performance. As shown in Figure 7, the ASALT Laboratory's optical bench contains both an SRI WFS and a Shack-Hartmann WFS. This allows for a versatile set of experiments comparing the performance of the two sensors as well as testing each sensor individually against various control parameters. Analysis comparing the performance of the SRI WFS and Shack-Hartmann WFS under various conditions is in progress. This paper discusses results of phase-shift approach and WFS resolution comparisons within the scope of SRI WFS performance only.

One of the ASALT Lab's main objectives is to provide flexibility and realistic, repeatable test scenarios.[4,8] The performance of the different phase-shift methods described in this paper was tested with the SRI wavefront sensor in the ASALT Laboratory. Analysis of the various methods continues to aid in determining the best method to use in a particular application. The remainder of this section describes the components of the ASALT Laboratory relevant to this study of phase-shift methods.

4.1 Atmospheric turbulence simulator

The Atmospheric Turbulence Simulator (ATS) allows laboratory tests to be performed in the presence of atmospheric-like turbulence.[8] The ATS consists of two phase wheels etched with Kolmogorov turbulence statistics. One phase wheel simulates a low atmospheric layer, while the other simulates high-altitude turbulence. Together, these plates are capable of providing a wide range of atmospheric conditions. Mechanical and optical positioning of the phase plates in the beam path control r_0 and σ_χ^2. Computer-controlled stepper motors rotate the phase wheels through the beam to vary the Greenwood frequency. In addition, because the computer controls rotational position and speed of the phase wheels, turbulence scenarios can be repeated for comparison of various parameters through a wide range of tests.

4.2 Deformable mirror

The aberrated beam leaves the ATS, is relayed to a steering mirror (SM), and then is relayed to the deformable mirror (DM). The SM and DM are both conjugate to the system pupil. The ASALT Lab DM is a Xinetics 577-channel continuous surface mirror with 8μm of physical stroke and 7.7 mm actuator spacing. At pupil, the beam is wide enough to accommodate 25 DM actuators (24 actuator spacings). While the DM can operate at several kilohertz, the system

frame rate is limited to a few tens of hertz due to PC sequential processing as well as the frame rates available from the use of commercial IR cameras from Indigo for the WFS and focal plane scoring cameras.

4.3 SRI WFS

Figure 7 shows the layout of the SRI WFS in the ASALT Laboratory. After reflection from the SM and DM, part of the beam is used for the beacon, and part is coupled into a single mode fiber to form the SRI WFS reference. About 10% of the fiber-coupled power is measured by a photodiode to determine coupling efficiency and on-axis Strehl ratio of the corrected beam. The other 90% of the fiber power is used for the reference. Components in the fiber path include an optical isolator, a semiconductor optical amplifier (SOA), a fiber phase shifter, and a narrow-band (0.3 nm) spectral filter. The isolator ensures that no amplified spontaneous emissions (ASE) propagate back through the system and cause problems with the input laser source or other detectors in the layout. The spectral filter blocks out-of-band ASE in the reference beam. At the output of the fiber path, a lens collimates the reference so it can be recombined with the beacon beam on the SRI WFS camera.

4.4 Current phase-shift implementation

The SRI WFS currently uses temporal phase shifting accomplished with an inline fiber phase shifter. Hardware implementation of a spatial phase shifter is currently being fabricated. However, any of the phase-shifting approaches described above can be implemented in software by the computer control system. The ASALT control system provides a well-defined, flexible architecture for integrating and linking hardware and software elements. The user can build anything from simple calibration layouts to complex, closed-loop AO systems and run them from the control console. Figure 8 shows a layout designed to test closed-loop, spatial-temporal phase shifting using a high resolution SRI WFS. Components on the optics table are represented by components in the control console (denoted by gray boxes in Fig. 8). Control console components also include software processing nodes such as the SRI Real-Time Reconstructor (RTR). The control console drives the AO loop, synchronizes component operation, and records data for WFS performance analysis.
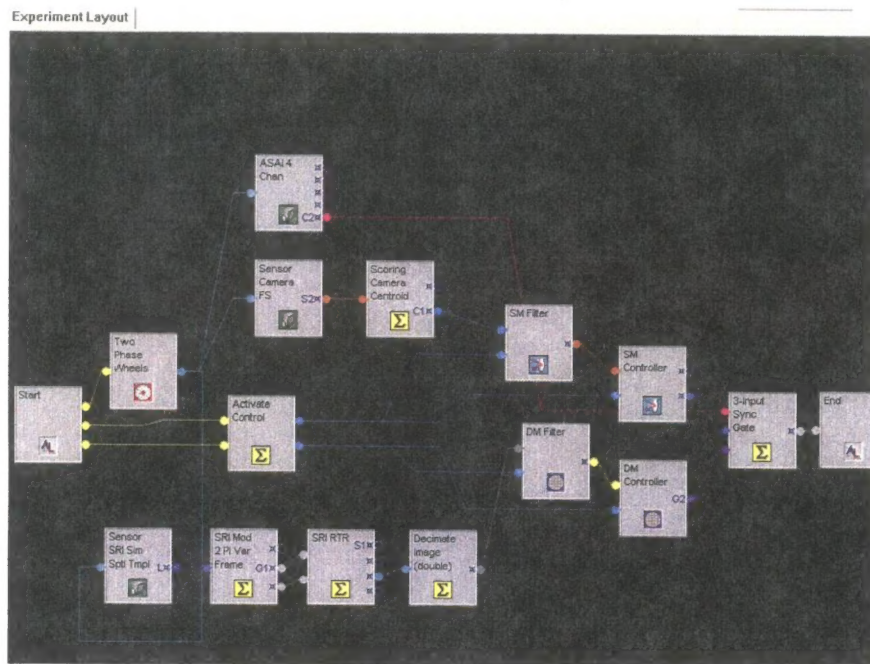

Figure 8. Screen capture of ASALT Control Console layout for spatial-temporal phase shifting with 49x49 subaperture resolution. Gray boxes denote hardware and software components, i.e. camera frame sources, stepper motor control for phase wheels, DM and SM controllers, SRI RTR, and component operation synchronization. Components are linked to pass data through the system.

Because the computer has control and synchronizes component operations, it can "freeze" time, pause the stepper motors to stop the ATS phase wheels from turning, and take multiple WFS images at one simulated instant in time. As a result, spatial phase shifting can be simulated because each of the four phase shifts produced by the fiber phase shifter will be imaged through the exact same turbulence pattern, just as if the original beam from one instant in time had been split four ways in space and imaged. Likewise, spatial-temporal phase shifting can be simulated as the control system freezes time to image each of the two phase shifts produced by the fiber phase shifter through the same turbulence setting. As time is advanced one step, the fiber phase shifter then produces the next two images through the next turbulence setting to complete the series of four images.

The main limitation of this simulation method is that the hardware challenges of spatial phase shifting, namely calibration and alignment, are not accurately simulated. In the experiments presented below, the same camera pixels are used for all of the spatial images, whereas four separate detector arrays would be present in a true spatial phase-shifting system. Furthermore, the beam strength is twice what it should be as the beam is split only twice rather than four times. This could have been mitigated by turning down the power for these simulations, though the illumination was high enough that this should have not had a significant impact on performance. The capability to add artificial gain and offset noise is under development, but was not implemented in time to include in these experiments. This capability will allow for more accurate simulation of more than one detector array. In addition to simulation, the hardware implementation of the spatial phase shifter under development will augment the realistic phase-shift testing capabilities of the ASALT Lab.

5. TEST RESULTS

We performed tests in the ASALT Laboratory to compare phase-shift methods at two WFS resolutions. Table 1 shows the atmospheric scenarios used. The first three scenarios were used to compare performance as a function of phase-shift method and WFS resolution over a range of turbulence conditions. The fourth scenario was used to compare phase-shift method performance as a function of Greenwood frequency using a high-resolution SRI WFS only.

#	d_{act}/r_0	Rytov σ_χ^2
1	0.27	0.11
2	0.41	0.36
3	0.50	0.57
4	0.44	0.42

Table 1. Atmospheric turbulence scenarios used for testing. Scenarios 1-3 were used to compare phase-shift methods and WFS resolution. Scenario 4 was used to compare phase-shift methods as a function of Greenwood frequency.

To appropriately compare WFS performance, the ATS was set back to the same starting point for every data set collected. Only one atmospheric realization with 250 frames of data was collected for each data set. Tracking was initiated at frame 25 and the higher-order AO loop was activated at frame 50. Fifty additional frames were allotted to allow time for the loop to close and reach a steady-state regime. Consequently, average system Strehl was calculated by using the last 150 scoring images from the data set. System Strehls were calculated relative to a reference point spread function (PSF) obtained prior to introducing turbulence into the system. This reference PSF was collected by sending a clean, unaberrated beam into the optical path of the scoring sensor. The reference Strehl represents the best Strehl that the SRI WFS could achieve with the specific laboratory optical setup. The sliding window method was used to reconstruct the wavefront aberrations in the spatial-temporal and temporal methods.

Figure 9 shows the results of Scenarios 1-3 comparing the different phase-shift methods. Fig. 9a shows results for a high-resolution WFS (49x49 subapertures) and Fig. 9b shows results for a low-resolution WFS (25x25 subapertures). For both resolutions, as turbulence increased, Strehl decreased. The figures plot Strehl as a function of the Rytov number but, as shown in Table 1, r_0 increased as σ_χ^2 increased. While Section 2 described how the SRI WFS is theoretically immune to scintillation, the Strehls shown in Fig. 9 are system Strehls that include not only WFS accuracy, but also DM fitting error, system latency, misalignments, and other noise contributions. It is expected that system Strehl

will decrease with increasing turbulence and will not be immune to scintillation. In the near future, we are looking to compare these results to theory laid out in previous work.[6]
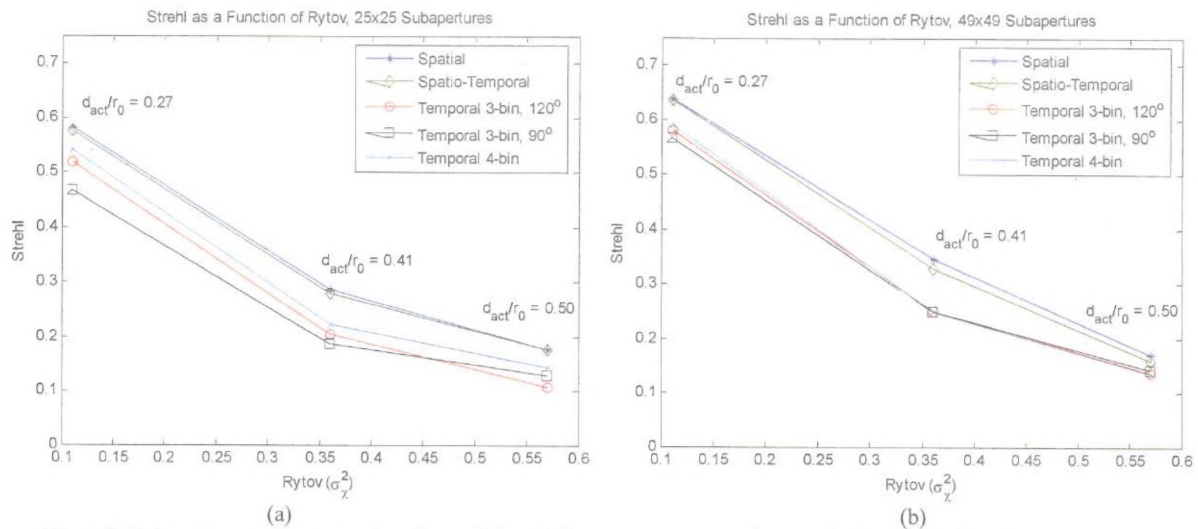

Figure 9. Laboratory results comparing phase-shift techniques over a range of atmospheric scintillations (i.e., scenarios 1-3 in Table 1). (a) WFS resolution is 25x25 subapertures. (b) WFS resolution is 49x49 subapertures. As σ_χ^2 increased, r_0 increased as well. At weaker turbulence, performance is slightly better with higher resolution.

The performance of the high and low resolution SRI WFSs were very similar, though the high-resolution performance was slightly better at weaker turbulence. The close similarity was a bit unexpected, but as described in Section 3.6, DM fitting could have become a significant factor in system performance. The high-resolution WFS may have produced more accurate measurements than the low-resolution WFS, but it may not have achieved the full potential of high-resolution while constrained to use the same number of DM actuators as the low-resolution WFS. DM fitting and WFS accuracy may also have been factors in the different temporal results obtained from each resolution. The low-resolution WFS results show the performance of the temporal methods more spread out than in the high-resolution results.

Comparing the phase-shift methods for both WFS resolutions, spatial and spatial-temporal phase shifting show noticeably better performance than the temporal methods. While we expect the spatial method to perform better than all others since it is not affected by the changing atmosphere, in the realization studied, the spatial method performs only slightly better than the spatial-temporal method. We would expect the spatial-temporal method to perform about half way between spatial and temporal, yet this is not the case. Perhaps this indicates that the trade-offs between the spatial and temporal methods do not yield a 50-50 balance. Another possibility is that because the spatial phase shifting tested in the laboratory was simulated rather than implemented in hardware, some latency effects could have drifted into the system. However, as discussed earlier, simulating the spatial phase shifting has excluded the complication of spatial alignment and calibration, and these simulation effects may have balanced each other out.

The temporal methods in the high-resolution WFS results show very similar performance, although, in the low-resolution WFS case, they are more spread out. In these results, the 4-bin method performs somewhat better than the 3-bin methods. Since the 4-bin method is less susceptible to noise while the 3-bin method has a lower latency, this could indicate that noise is a more dominant factor than latency in this particular atmospheric realization. At weaker turbulence, the 3-bin method with 120-degree phase shifts performs somewhat better than the 3-bin method with 90-degree phase shifts. This trend is expected because the 120-degree spacing allows for complete sampling of the unit circle where 90-degree spacing allows for sampling only ¾ of the circle. However, it should be noted that these results are not comprehensive, as the difference in performance between these methods is small and only one atmospheric realization was implemented. Furthermore, the wider spread of temporal phase-shift performance results in the low-

resolution case could be due to lower WFS measurement accuracy as described above. Finally, the ordering of the phase shifts in the temporal methods may be a factor that contributes to performance. However, that was not tested in these experiments. We hope to examine this issue in future testing.

Scenario 4 compared phase-shift method performance as a function of Greenwood frequency. Tracking, AO loop closure, and Strehl calculation were performed as described above for Scenarios 1-3. However, only the high-resolution SRI WFS was used as the experiment objective focused on the speed of the atmospheric turbulence, and either resolution would have produced the same general trends. To increase Greenwood frequency, the speed of the phase wheels was increased in the ASALT control console with each successive test. Therefore, while each atmospheric realization began at the same point, the realizations changed as phase wheel speed increased and "new" turbulence entered the system at the end of each run. However, the set of realizations was identical for each phase-shift method. Figure 10 shows the results of this experiment.
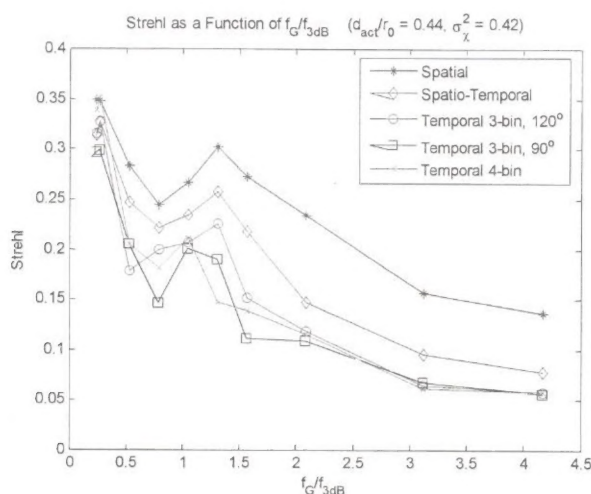

Figure 10. Strehl vs. Greenwood frequency for each phase-shift method in moderate turbulence (scenario 4). The spatial method performs the best, as expected. At slower speeds, the spatial-temporal method performs similarly to the spatial method, but at faster speeds, its performance drops as in the temporal methods.

As f_G increased, Strehl decreased for all phase-shift methods. This is to be expected as each method must compensate for a more rapidly shifting atmosphere. However, as Greenwood frequency increased, the performance of the spatial-temporal and temporal methods decreased noticeably faster than the performance of the spatial method. This is to be expected due to the dynamic nature of the atmospheric turbulence encountered between measurements as well as to the latency in updating the DM inherent in temporal methods.

The dip in Strehl for all phase-shift methods between an f_G/f_{3dB} of 0.5-1.0 may result from the particular atmospheric realization used. The phase wheels simulate only a two-layer atmosphere and the system may have encountered a particularly strong turbulence scenario in this region. This is probable especially because every method shows the same trend. Spurious lab turbulence or other noise contributions may not have caused such a consistently unexpected trend.

As expected, the spatial method showed the best Strehl performance. Because it is immune to dynamic turbulence shifts within a measurement period, the increasing Greenwood frequency did not degrade its performance to the extent that it degraded the performance of the temporal methods. As described above, the spatial-temporal method performed similarly to the spatial method at lower frequency, but its performance dropped rapidly and approached that of the temporal methods at higher frequency. This suggests that the temporal effects of the dynamic atmosphere are non-linear, and that the temporal nature of the measurement dominated at higher frequency. At the same time, the spatial-temporal method performed consistently and noticeably better than the strictly temporal methods, demonstrating that the spatial element still improves the method's overall performance compared to temporal.

While the temporal methods demonstrated similar trends as in the previous experiment, they were more variable, with the best performance switching between the three methods. This may be due to the new turbulence introduced with the changing realizations. Each method may have compensated for the new realizations differently. Furthermore, the ordering of the phase shifts in each temporal method may have been significant, as suggested above. At high frequencies, the differences between the temporal methods' performance washed out. At this high frequency, the system may have reached an effectively "open loop" regime. Correlation of this wash-out regime and open-loop Strehl will be performed in the future. In addition, tests will be performed to determine the significance of varying the order of the temporal phase shifts.

6. CLOSING COMMENTS

This paper examined the operation of the SRI WFS in reference to various phase-shifting techniques. The methods of spatial, temporal, and spatial-temporal phase shifting and trade-offs between them were explained. Components and test-setup in the ASALT Laboratory were presented. Finally, this paper described results from laboratory experiments that were performed to compare achieved system Strehls with each phase-shift technique while varying atmospheric conditions and WFS resolution.

Laboratory results showed that in comparing WFS resolution, increasing scintillation, and increasing Greenwood frequency, spatial phase shifting performed the best out of the phase-shift techniques studied. While spatial-temporal phase shifting performed very similarly to the spatial method regardless of scintillation strength, the spatial method performed considerably better than all other methods at high Greenwood frequencies. Temporal phase-shift methods consistently performed below the spatial and spatial-temporal methods. These results indicate that the effects of dynamic turbulence are indeed significant in achievable system Strehl. Performance drawbacks of using temporal phase shifting must be weighed against the cost and complexity of implementing spatial phase shifting. Employing spatial-temporal phase shifting may therefore become a desirable compromise.

Further experimentation will be performed to determine how to improve the performance of each phase-shift method. Future work will include calculation of the branch-point contributions in phase unwrapping. In addition, a hardware implementation of a spatial phase shifter is in fabrication and will allow direct determination of spatial phase-shift performance without relying on simulation. With a mechanical spatial phase shifter, a more accurate comparison of the trade-offs between spatial and temporal methods will be possible. Temporal phase-shifting analysis will include an investigation into the significance of the order of temporal phase shifts as well as a comparison of sliding window versus non sliding window methods for reconstructing the wavefront aberrations. Finally, future work will include a wider range of atmospheric realizations and comparison of laboratory results to theory.

REFERENCES

1. J. D. Barchers, D. L. Fried, and D. J. Link, "Evaluation of the performance of Hartmann sensors in strong scintillation," *Appl. Opt.* **41**, pp. 1012-1021, 2002.
2. J. D. Barchers, D. L. Fried, and D. J. Link, " Evaluation of the performance of a shearing interferometer in strong scintillation in the absence of additive measurement noise," *Appl. Opt.* **41**, pp. 3674-3684, 2002.
3. J. D. Barchers, D. L. Fried, D. J. Link, G. A. Tyler, W. Moretti, T. J. Brennan, and R. Q. Fugate, "Performance of wavefront sensors in strong scintillation," *Proc. SPIE* **4839**, pp. 217-227, 2003.
4. T. A. Rhoadarmer, "Development of a self-referencing interferometer wavefront sensor," *Proc. SPIE* **5553**, pp. 112-126, 2004.
5. T.A. Rhoadarmer and J.D. Barchers, "Noise analysis for complex field estimation using a self-referencing interferometer wave front sensor," *Proc. SPIE* **4825**, pp. 215-227, 2002.
6. J. D. Barchers and T.A. Rhoadarmer, "Evaluation of phase-shifting approaches for a point-diffraction interferometer with the mutual coherence function," *Appl. Opt.* **41**, pp. 7499-7509, 2002.
7. D. Malacara, *Optical Shop Testing*, Wiley, New York, 1992.
8. S. V. Mantravadi, T.A. Rhoadarmer, "Simple laboratory system for generating well-controlled atmospheric-like turbulence," *Proc. SPIE* **5553**, pp. 290-300, 2004.